3

Development of Sintered MCrAlY Alloys for Aeronautical Applications

Fernando Juárez López and Ricardo Cuenca Alvarez
Instituto Politécnico Nacional-CIITEC
México

1. Introduction

Thermal barrier coatings (TBCs) are widely used in turbines for propulsion and power generation (Bose & DeMasi-Marcin ,1995; Choi et al., 1998; Cruse et al. 1988; DeMasi-Marcin & Gupta, 1994; DeMasi-Marcin et al., 1990; Eaton & Novak, 1987; Golightly et al., 1976; Hillery, 1996; Lee & Sisson, 1994; Mariochocchi et al., 1995; Meier et al. ,1991 & Gupta, 1994; Miller, 1984; Kingery et al., 1976; Rigney et al., 1995; Strangman, 1985; Stiger et al., 199;, 1999 & Evans, 1999). They comprise thermally insulating materials having sufficient thickness and durability that they can sustain an appreciable temperature difference between the load bearing alloy and the coating surface. The benefit of these coatings results from their ability to sustain high thermal gradients in the presence of adequate back-side cooling. Lowering the temperature of the metal substrate prologs the life of the component: whether from environmental attack, creep rupture, or fatigue. In addition, by reducing the thermal gradients in the metal, the coating diminishes the driving force for thermal fatigue. Both of these benefits can be traded off in design for greater component durability, or for reduced cooling air or for higher gas temperature/improved system efficiency. As a result, TBCs have been increasingly used in turbine engines. Successful implementation has required comprehensive testing protocols, facilitated by engineering models (Cruse et al. 1988; Eaton & Novak, 1987; Meier et al. ,1991; Wright, 1998). Expanded application to more demanding scenarios (Fig. 1) requires that their basic thermo-mechanical characteristic be understood and quantified. This need provides the opportunities and challenges discussed in this article.

There are four primary constituents in a thermal protection system (Fig. 2). They comprise (i) the TBC itself, (ii) the superalloy substrate, (iii) an aluminum containing bond coat (BC) between the substrate and the TBC, and (iv) a thermal grown oxide (TGO), predominantly alumina that forms between TBC and the BC. The TBC is the insulator, the TGO on the BC provides the oxidation protection and the alloy sustains the structural loads. The TGO is a reaction product. Each of these elements is dynamic and all interact to control the performance and durability.

The thermal barrier coating is a thermally insulating, “strain tolerant” oxide. Zirconia has emerged as the preferred material, stabilized into its cubic/tetragonal forms by the addition of Yttria in solid solution. This material has low thermal conductivity (~1 W/m^2) with

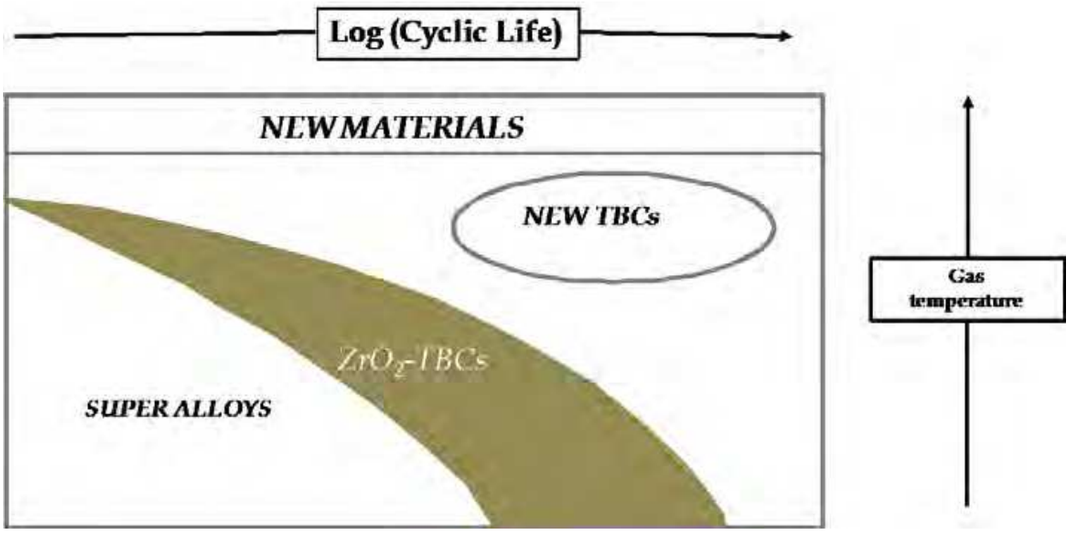

Fig. 1. Schematic indicating the operating domain for TBCs and the challenge for a new generation of materials.

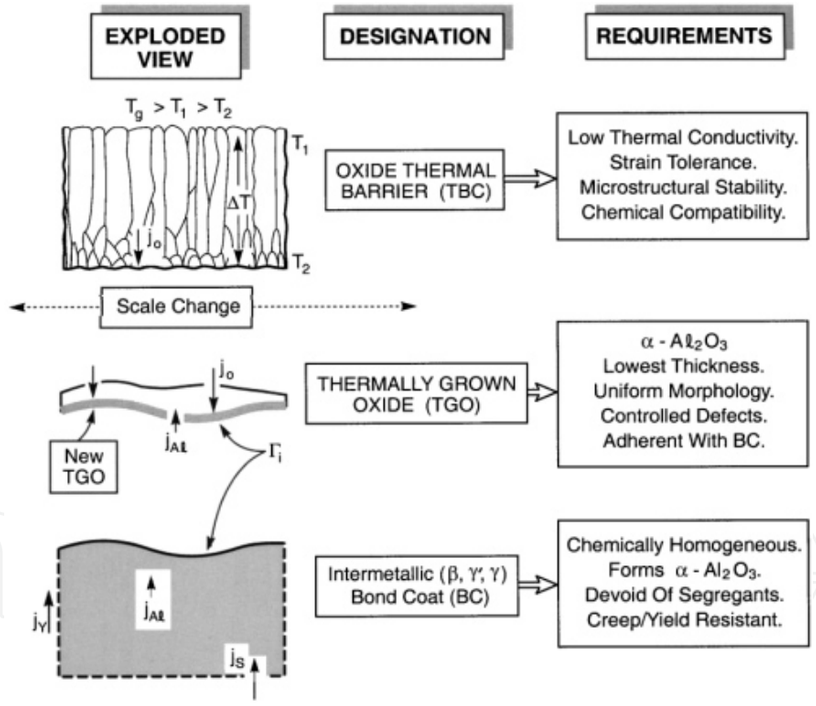

Fig. 2. The four major elements of a thermal barrier system: each element changes with exposure / cycling.

minimal temperature sensitivity (Fig. 3) (Kingery, 1976). The thermal resistance at lower temperatures corresponds to a phonon mean free path governed by structural vacancy scattering. Complex oxides having even lower conduction are being investigated, but there is not affirmation of their viability as TBCs. Strain tolerance is design into the material to avoid instantaneous delamination from thermal expansion misfit. Two methods are used to

deposit strain tolerant TBCs. Electron beam physical vapor deposition (EB-PVD) evaporates the oxide from an ingot and directs the vapor onto the preheated component (Hillery, 1996; Mariochocchi et al., 1995; Rigney et al. 1995). The deposition conditions are designed to create a columnar grain structure with multiscale porosity (Fig. 2) that provides the strain tolerance and also reduces the thermal conductivity (to about 0.5 W/m K, Fig. 3). Air plasma spray (APS) deposition is a lower cost alternative (DeMasi-Marcin et al. 1990; Lee & Sisson, 1994; Choi et al., 1998). The deposition is designed to incorporate intersplat porosity and a network of crack-like voids that again provides some strain tolerance, while lowering the thermal conductivity.

The thermally grown oxide has a major influence on TBC durability (Cruse et al. 1988; Eaton & Novak, 1987; Golightly et al., 1976, Meier et al. ,1991; Stiger et al., 1999; Quadakkers et al., 1999; Wright, 1998, 1999). The bond coat alloy is design as a local Al reservoir (Fig. 2), enabling α- alumina to form in preference to other oxides, as oxygen ingresses through the TBC (which is transparent to oxygen).

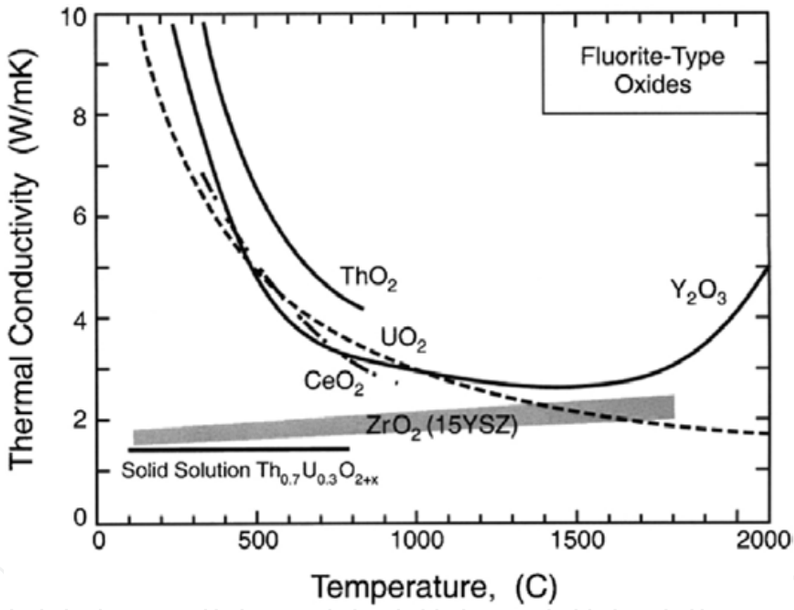

Fig. 3. The thermal conductivity of several insulating oxides illustrating the major role of solid solutions in affecting phonon transport (Evans et al., 2001).

Alumina is the preferred oxide because of its low oxygen diffusivity and superior adherence. This layer develops extremely large residual compressions (3-6 GPa, Fig. 4), as the system cools to ambient, primarily because of its thermal expansion misfit with the substrate (Fig. 5, Table 1) (Christensen et al., 1997; Lipkin & Clarke, 1996; Mennicke et al., 1997; Sarioglu et al. 1997; Sergo & Clarke, 1998; Tolpygo & Clarke, 1998, 1998). Stresses also arise during TGO growth (Lipkin & Clarke, 1996; Quadakkers et al., 1999; Stiger et al., 1999). They are much smaller (generally less than 1 GPa), but still important. Though thin (3-10 um), the high energy density in the TGO motives the failure mechanisms.

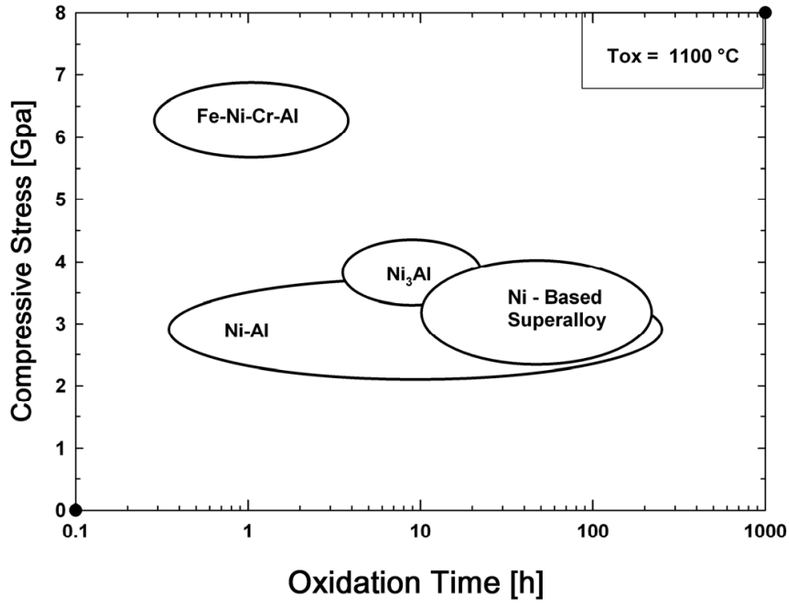

Fig. 4. Ambient residual compressions measured in the TGO developed on several alloy system (after (Lipkin & Clarke, 1996).

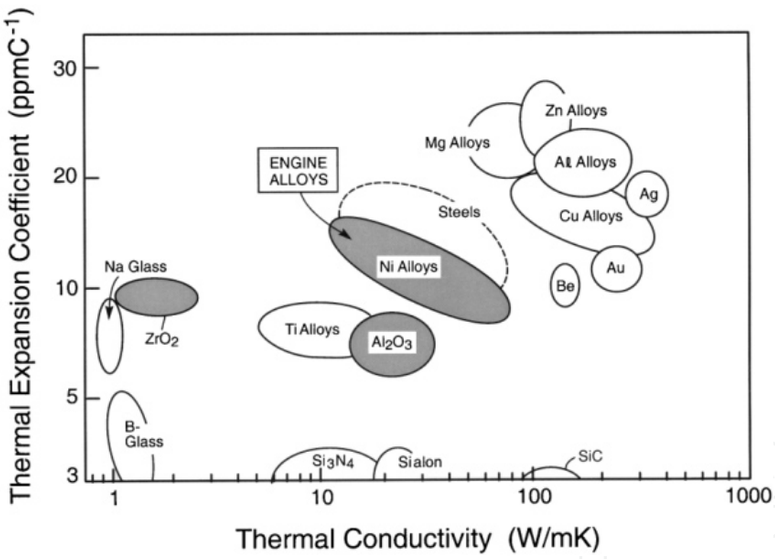

Fig. 5. Cross plot of the thermal expansion coefficient and thermal conductivity of the major materials constituents in the TBCs system (Evans et al., 2001).

The **bond coat** is arguably the most crucial component of the TBC system. Its chemistry and microstructure influence durability through the structure and morphology of the TGO created as it oxidizes (Stiger et al., 1999). Moreover, system performance is linked to its creep and yield characteristics. Bond coats are in two categories. One is based on the **NiCoCrAlY (MCrAlY**) system, typically deposited by low-pressure plasma spraying (LPPS). It is usually two-phase (β-NiAl and either γ - Ni solid solution or γ′-Ni_3Al). The γ/γ′ phases have various other elements in solution. The Y is added at low concentrations to improve the adhesion of the

TGO, primarily by acting as a solid state gettering site for S (Haynes, 1999; Meier & Pettit, 1999; Smegil, 1987; Smialek et al., 1994), which diffuses up from the substrate. In some cases, small amounts of a Ni-Y intermetallic may also be present. The second category consists of a Pt-modified diffusion aluminide, fabricated by electroplating a thin layer of Pt onto the superalloy and then aluminizing by either pack cementation or chemical vapor deposition. These coatings are typically single-phase-β, with Pt in solid solution (Stiger et al., 1999). Their composition evolves during manufacture and in-service. Diffusion of Al into the substrate results in the formation of γ´ at β grain boundaries (Stiger et al., 1999).

TGO (α-Al_2O_3)	
Young´s Modulus, E_o (GPa)	350-400
Growth stress, σ^g_{xx} (GPa)	0 – 1
Misfit compression, σ_0 (GPa)	3 – 4
Mode I fracture toughness, Γ_0 (J m^{-2})	20
Thermal expansion coefficient, α_o (C^{-1} ppm)	8 – 9
Bond coat	
Young´s modulus, E_s (GPa)	200
Yield strength (ambient temperature) σ_Y (MPa)	300-900
Thermal expansion coefficient, α_s (C^{-1} ppm)	13-16
Interface (α - Al_2O_3/bond coat)	
Mode 1 adhesion energy, Γ^0_1 (J m^{-2})	
Segregated	5-20
Clean	>100
TBC (ZrO_2/Y_2O_3)	
Thermal expansion coefficient, α_{tbc} (C^{-1} ppm)	11-13
Young´s modulus, E_{tbc} (GPa)	0-100
Delamination toughness T_{tbc} (J m^{-2})	1-100

Table 1. Summary of material properties.

The interface between the TGO and Bond coat is another critical element. It can be embrittled by segregation, particularly of S (Haynes, 1999; Meier & Pettit, 1999; Smegil, 1987; Smialek et al., 1994). During thermal exposure, S from the alloy migrates to the interface. Dopant elements present in the BC getter much of this S and suppress (but not eliminate) the embrittled. As already noted, bond coat based on NiCoCrAl contain Y for this purpose. The Pt-aluminide BCs do not contain elements which getter S. Nevertheless, they are durable and can have longer lives in cyclic oxidation than NiCoCrAlY systems Meier & Pettit, 1999). While it has been proposed that the Pt mitigates the effects of S [30], there is no fundamental reason to expect this. A number of effects of the Pt on the behavior Pt-modified aluminides have been documented (Schaeffer, 1988). But a complete understanding of the "Pt effect" is an important goal for future research.

A system approach to TBC design and performance requires that several basic bifurcations be recognized and characterized. Three of the most important are addressed.

i. The NiCoCrAlY and Pt-aluminide bond coats result in distinct TGO characteristics as well as differing tendencies for plastic deformation. Accordingly, the failure mechanisms are often different.

ii. TBCs made by APS and EB-PVD are so disparate in their microstructure, morphology and thermo-physical properties that different failure mechanisms apply.
iii. The failure mechanisms may differ for the two predominant areas of application (propulsion and power generation), because of vastly different thermal histories. Systems used for propulsion and for power peaking experience multiple thermal cycles, whereas most power systems operate largely in an isothermal mode with few cycles. The frequency affects coating durability.

Then NiCoCrAlY (MCrAlY) alloys are subjected to extensive research efforts to develop applications in gas turbine due to their high specific young's modulus and strength, and to their good oxidation and corrosion resistances. However, such alloys suffer from limited ductility at room temperature and creep resistance at service temperature (950- 1100°C) (Czech et al., 1994; Nickel et al., 1999; Monceau et al., 2000; Van de Voorde & Meetham, 2000). From a technological point of view, the current limitations are due to a large scattering in mechanical properties resulting from correlated chemical and structural heterogeneities, to manufacturing difficulties and high costs. In this context, the present work aimed to produce MCrAlY alloys with refined and homogenous microstructure by using the spark plasma sintering process (SPS) and hot pressing.

Indeed the need for improved oxidation and hot corrosion resistance of the protective oxide scale led to doping of the different bond coats by various metals like HF, Ir, Pd, Pt, Re, Ru, Ta, Zr (Alperine et al. 1989; Czech et al., 1994, 1995; Taylor & Bettridge, 1996) These, as well as other reports that have been published in the open and in the patent literature, (Taylor et al., 1995) conclude that doping of the bond coats by such elements was globally beneficial. However, for plasma-sprayed MCrAlY bond coats, the difficulty of performing such an investigation may be due to the cost of the dopants associated with the relatively large quality of powder required for the coating operation, even if it is performed on the laboratory scale, or to the mixing process involving either alloying high melting temperature elements or mechanical mixing with possible contamination from the atmosphere and the mixing apparatus.

A solution to this problem could be an economic, versatile, and time saving process allowing the doping of quantities of commercially available material with well established performance. The reference and doped powders could then be used for the preparation and compaction samples to produce the bond coat. These samples could, in turn, be subjected to thermal and cyclic oxidation and corrosion test, followed by adhesion test of the superficial scale that is produced.

In this sense a collaborative program was currently underway to satisfy this need. The process being investigated is superficial doping of commercially available MCrAlY powders which are actually used in industry, with Ruthenium as a series of platinum group metals, using the SB-MOCVD (Spouted Bed Metal-Organic Chemical Vapour Deposition) technique. In contrast to the direct mixing of the MCrAlY powder with the additive, this process ensures homogeneous distribution of the metallic additives on the surfaces of each particle and, consequently homogeneous distribution of the doping elements throughout the volume of the bond coats (Juarez et al., 2003). Initial results introducing the SB-MOCVD doped process have presented in (Caussat et al., 2006; Juarez et al., 2001; Vahlas et al., 2002).

The choice of Ruthenium (Ru) and Rhenium (Re) for this study is based on recent results, following which doping of monocrystalline nickel superalloys with this element reduces their high-temperature creep (Feng et al., 2003; Fleischer, 1991; Lu & Pollock, 1999, 1999; Noebe et al., 1993; Pollock et al., 2001; Tryon, 2006; Tryon et al., 2004; Wang et al. 2011; Wolff, 1997; Wolff, & Sauthoff, 1996).

In this context, the present study aimed to produce MCrAlY alloys with refined and homogenous microstructure by using the uniaxial hot pressing and spark plasma sintering process (SPS).

Then, firstly MCrAlY powders were doped by Ru and Re. The doping level, purity, microstructure and, Ru and Re distribution of the powders were established. TEM samples of Ru and Re nanometric coatings on the surfaces MCrAlY particles are presented. They allowed the investigations of morphology, the microstructure and the composition of the Ru-coatings. Second, at moment of this manuscript Ru-doped MCrAlY and undoped MCrAlY powders were sintered at 1473 K by only uniaxial hot pressing. Finally, MCrAlY undoped powders were sintered by SPS.

2. MCrAlY powder characteristics

The commercial MCrAlY powder is a pre-alloyed material, which is mainly composed of Ni with additions of Co (21 wt.%), Cr (19 wt.%), Al (8 wt.%), Y (1 wt. %) and Ta (5 wt.%). Fig. 6a shows a SEM micrograph of the as-received powder featuring spherical shape and agglomerates. Their skeleton-like shape report a theoretical density of 7700 kg/m^3, while the apparent tap density is 4300 kg/m^3. Specific surface area was computed from the N_2 adsorption isotherms (recorded at -196 ^{o}C with a Micrometrics Flowsorb II2300), using the BET method and was found to be 0.83 m^2/g. This low value is characteristic of a non porous material. Powder size distribution was determined with a Malvern Mastersizer laser diffractometer. It was found that mean size distribution of the particles is 23 µm, with minimum 0.05 µm and maximum 556 µm. Fig. 6b presents the particle size distribution measurement of the MCrAlY superalloy.

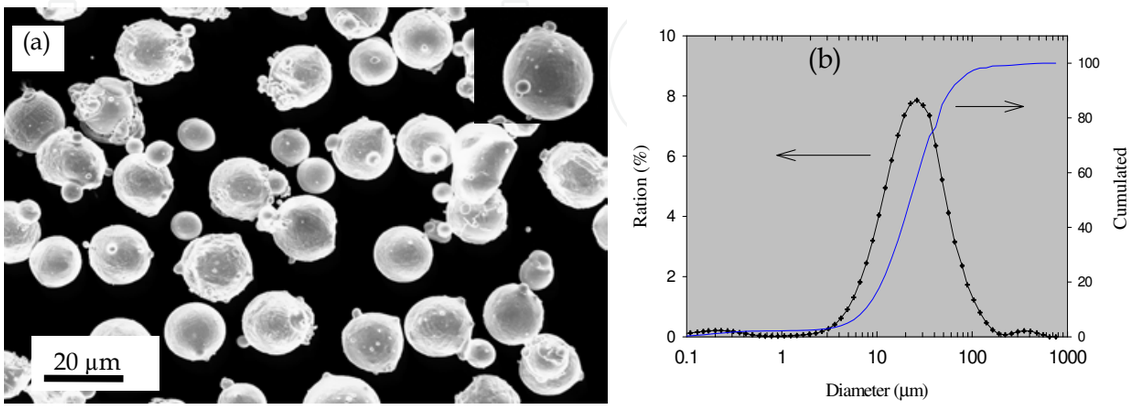

Fig. 6. Scanning electron micrograph of the as-received powders illustrating the spherical morphology and small agglomerated (a). Particle size distribution measured of the MCrAlY powder (b).

3. MCrAlY doped

We used a spouted bed reactor in a research program aiming the superficial doping with ruthenium and rhenium of as received commercial powders of MCrAlY alloys by MOCVD (Caussat et al., 2006; Juarez et al., 2001, 2005; Vahlas et al., 2002). Our results revealed that; since the uniform modification of the composition of commercial raw material is possible by SBMOCVD, the end user could dispose of a valuable tool to adjust the properties of use as a function of the aimed application. However, to end the validation of this process for the wanted application, the hydrodynamic behavior of such peculiar powders in a lab-scale SB contactor remained to be studied.

3.1 Characteristics MCrAlY powder doped

3.1.1 SEM analysis

The evolution of materials science towards nanometric scales requires appropriate microstructure characterization techniques and the corresponding specimen preparation. Correlating the processing conditions, in terms of both the quality of spouting (coat and MOCVD) and the efficiency of the MOCVD, with the oxidation resistance required an insight into the nature and the morphology of typically 50 nm thick films deposited on the surface of particles with a mean diameter of 25 um.

The positive results validated the use of a SB for the superficial doping by Ru and Re of MCrAlY powders by MOCVD. It allowed homogenous deposition of the two metals on the surface of the MCrAlY powder.

The morphology of the Re and Ru films, on the surface of MCrAlY powders is shown in the SEM micrographs of Fig. 7. The Ru films were deposited in the presence of SB-MOCVD.

EDS maps of the corresponding elements are also presented. Re and Ru films are uniforms and their morphology is smooth. Deposition of Ru is efficient on the entire available surface of the particles in contrast to Re which covers only parts of the particle.

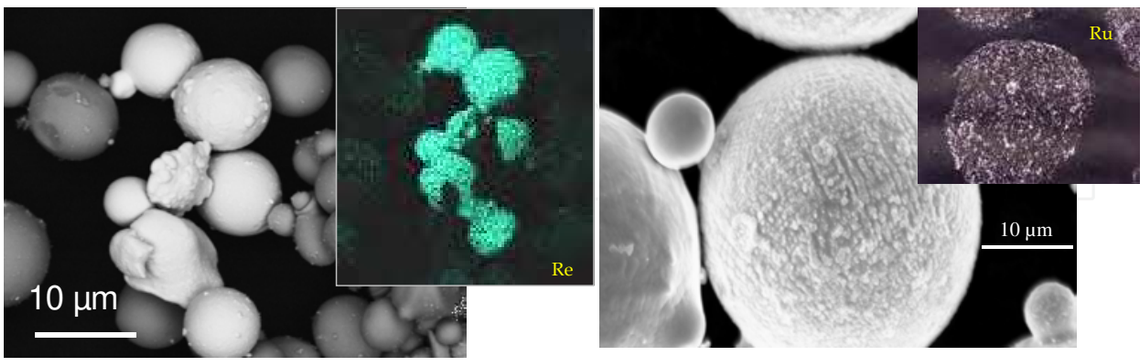

(a) (b)

Fig. 7. Secondary electrons SEM micrograph of MCrAlY powders with Re (a) and Ru (b) deposited on their surface, and corresponding EDS maps.

The SEM images in the Fig. 8 show the Ru deposit on a particle. The secondary electron micrograph on the left reveals a wrinkled surface morphology, compared to the smooth one

of the as-received powders, illustrated in the Fig. 8. This morphology is due to the Ru being deposited on the whole surface of the powders as shown in the EDS Ru map of the same particle, on the right. The doping level of the MCrAlY powders was, in this case, 0.8 wt. %.

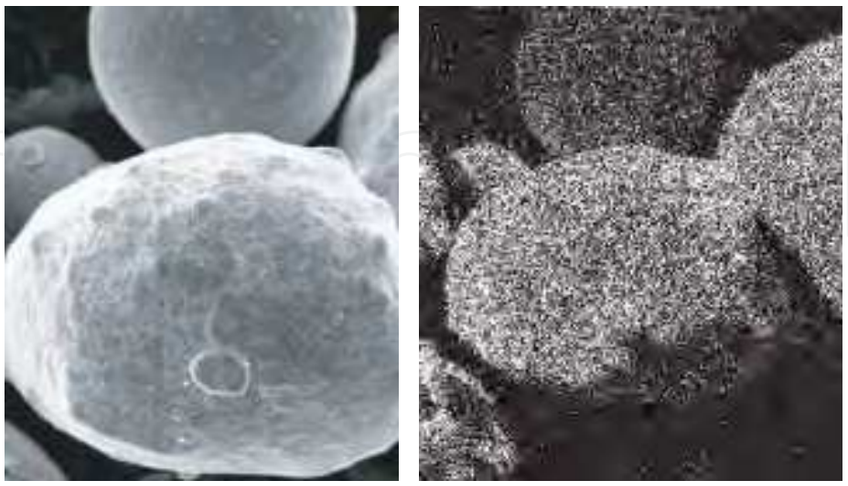

Fig. 8. SEM images of Ru deposited on MCrAlY powder. The micrographs are secondary electron (left) and Ru EDS mapping (Right) of a particle covered by Ru under adequate SB-MOCVD conditions.

3.1.2 TEM analysis

It is particularly important in transmission electron microscopy (TEM) observations of either thin areas in bulk materials such as interfaces in compositions, fine powder particles (Shiojiri et al., 1999; Yoshioka et al., 1996) or other complex in-shape samples (Yoshioka et al., 1995). The need to dispose of an appropriate TEM specimen preparation protocol was reported in our work for which 0.70 wt. % Rhenium (Re) and 0.90 wt. % Ruthenium (Ru) were added to the surface of commercial pre-alloyed MCrAlY powders (Caussat et al., 2006; Juarez et al., 2001, 2005; Vahlas et al., 2002).

The preparation of thin sections of Ru-doped powders was based on a method proposed by Yoshioka et al. (Shiojiri et al., 1999; Yoshioka et al., 1995, 1996). The sample was mixed with Gatan G1 epoxy resin in a Teflon cup and a drop of the suspension was placed on electron microscopy grid (100 mesh) that was positioned on a potassium bromide (KBr) crystal. It was aimed to obtain a sample that contained enough particles for convenient observation but not too much, to present satisfactory cohesion with enough resin. After polymerization of the epoxy at 373 K, the grid was wet-stripped from the KBr and mechanically polished with a South Bay Tech Tripod ® to reduce the overall thickness down to 70 um. The sample was finally ion-milled during 5-6 h in Gatan Precision Ion Polishing Systems (PIPS) equipment until a hole was detected. PIPS operating conditions were; acceleration voltage of the ion gun 5 keV, rotation frequency 3rpm, and incidence angle of the two ion beams on both sides of the sample 8-10 deg.

The above presented way to prepare cross section for TEM is rapid and relatively easy. However, it can only be used in the case of particles with a homogenously distributed deposit on their surface. As shown below, it was more difficult to localize the Re-containing

zones of the particle surfaces due to the less homogeneous distribution of Re than of Ru of the sample. In this case, the sample and G1 epoxy resin mixture was transferred to a brass tube whose internal diameter and wall thickness were 2.4 and 0.3 mm, respectively. After curing at 373 K the tube was sliced into a series of 300 um thick discs using a wire diamond saw. Finally, the discs were mechanically ground to a thickness of 100 um, and dimpled to about 40 um prior to ion thinning to electron microscopy transparency in the PIPS. At that time, the sample was very brittle and it was necessary to stick it to a specimen support grid with silver paste before the observation.

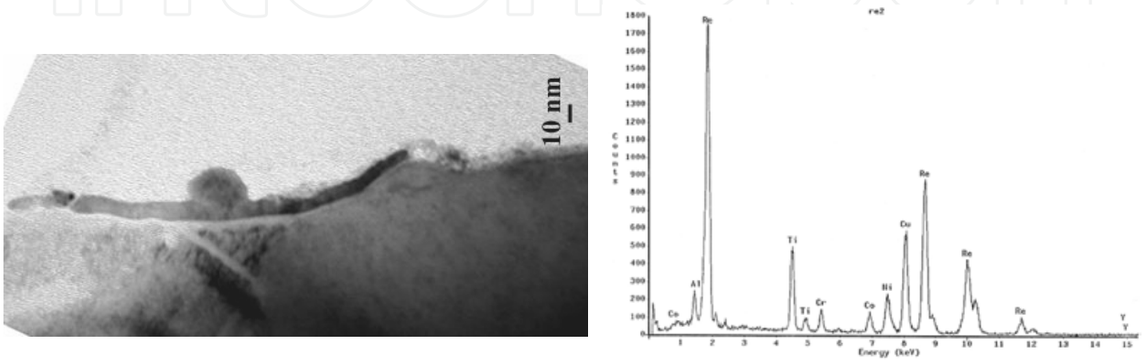

Fig. 9. Bright field TEM micrographs of the nanocrystallite Re coating on MCrAlY powder. Re cluster on the right of the micrograph reveals homogeneous side- nucleation.

Fig. 9 presents bright field TEM images of the nanocrystallite Re coating at two regions on MCrAlY powder. The film is continuous and its thickness varies between 10 and 40 nm. It is composed of particles typically sized around 10 nm. A larger cluster composed of Re grains is also shown in the micrograph. EDS revealed pure Re for both the film and the cluster.

Fig. 10 shows a dark field TEM micrograph of coating deposited from SB-MOCVD. The micrograph was obtained from an electron beam centered on the D1 and D3 spots of the corresponding EDP shown in the insert. The measured interplanar distances on this sample are also reported in Table 2. They reveal that the film is composed of pure crystalline Ru in agreement with X-Ray diffraction analysis.

	D (cm)	d_{exp} (nm)	Plan	$d_{JCPDS\ \#6\text{-}663}$
1	0,85	0,235	100	0,2343
2	1,0	0,211	002	0,2142
3	1,28	0,205	101	0,2056
4	1,68	0,157	102	0,1581
5	2,10	0,119	103	0,1219

Table 2. Interplanar distances of pure crystalline Ru.

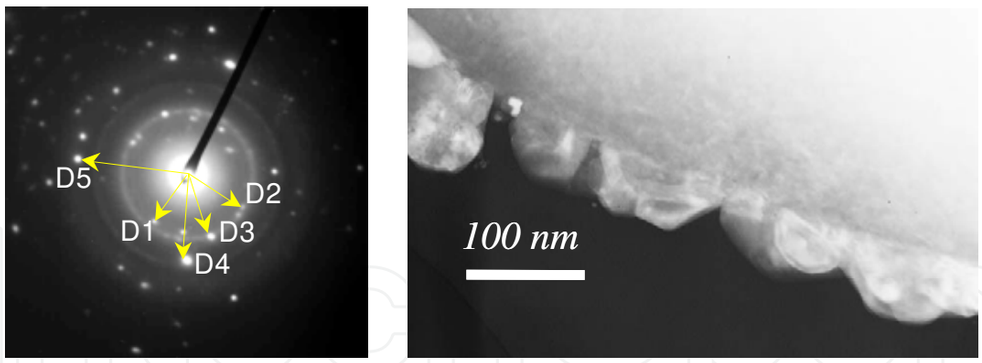

Fig. 10. Bright field TEM micrograph of Ru deposit and corresponding electron diffraction pattern.

Continuous Ru films deposited on the surface of MCrAlY particles are composed of the grains whose diameter approaches 100 nm. These grains are in turn composed of smaller crystallites. Fig. 11 illustrates this microstructure. In the Table 2 the interplanar spacing measured from the diffraction spots of Fig. 10 are presented and compared with the corresponding JCPDS values. Similar data from Ru samples, as presented in the following paragraphs are also included in this table.

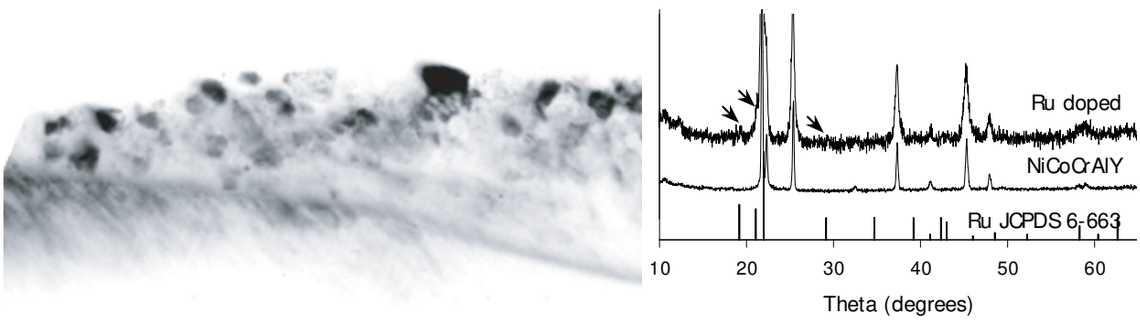

Fig. 11. Bright filed TEM image of Ru.

This parameter, together with the simplicity of this process should be considered for the final selection of the deposition route on the surface of MCrAlY powders of these, as well as other, metals.

4. Sintering of MCrAlY powders

4.1 Hot-pressing MCrAlY powders undoped and Ru-doped powders

Sintering of MCrAlY powder was carried out by uniaxial hot pressing at temperatures ranging between 1173 and 1473 K and during periods 0 to 60 minutes. The powders were poured into graphite dies coated with boron nitride and were sintered in a graphite furnace by uniaxial hot pressing. As shown below, this temperature is high enough: (i) to ensure densification of the samples; and (ii) to stabilize the microstructure in view of the subsequent heat treatments. A load pressure of 10 MPa is initially applied and the system operated under primary vacuum up to 523 K. Then, Ar flow was established and the pressure was gradually increased to achieve 40 MPa at 1273 K. During cooling, the pressure

was gradually decreased. Heating and cooling rates were 20 ^{o}C min^{-1}. Densification is practically up to 94%.

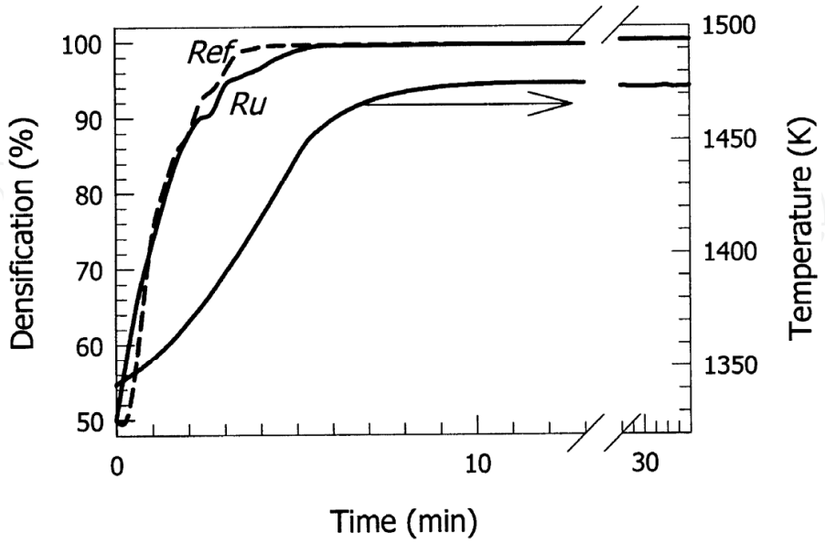

Fig. 12. Densification of the MCrAlY powders versus the duration of the uniaxial hot pressing performed at 1473 K. 100% densification corresponds to a pore-free sample.

Fig. 12 presents densification of reference and Ru-doped powders as a function of time for a temperature of 1473 K and during 30 min. Densification of both is practically identical up to 94%. During this period under the operating conditions used, grain boundaries were deformed and reorganized, especially due to the plastic deformation of the Al-rich b phase. Contact among surfaces is favored and the resulting product is exempt from open porosity. Elimination of closed porosity involves diffusion through grain boundaries and is somewhat slower in the doped sample. In view of this behavior, the same hot-pressing duration of 1 h was selected for both samples, ensuring complete densification and a similar microstructure.

The Fig. 13 (a) corresponds to the sintered sample at 1323 K, this micrograph shows characteristics of the powders in charge, where the powders present certain plasticity. Indeed, there is a pressure contact between faces of the powder due to the action mechanical exerted by the piston, consequently some powder boundaries begin to disappear. Intergranular diffusion starts but plasticity or diffusion rates do not contribute to the complete elimination of porosity. In practical the process is even slower in the periphery of the sample due to the frictional forces against the die walls and the slight contamination by boron nitride. An increase in the sintering temperature of 150 °C (1473 K Fig. 13 (c) micrograph) allowed an improvement of the densification but only after 60 min.

Fig. 14 presents a backscattered scanning electron micrograph of a polished surface of the Ru-doped sintered sample. Two phases, shown in dark and light gray, are present. They correspond to β-NiAl and to γ-Ni, respectively. White dots also appear in this micrograph; they correspond to tantalum carbide. The microstructure revealed is comparable to that of the corresponding bond coat applied by plasma torch in terms of the nature and distribution of the phases present. Consequently, the different properties of both materials, particularly their oxidation behavior, are also expected to be comparable.

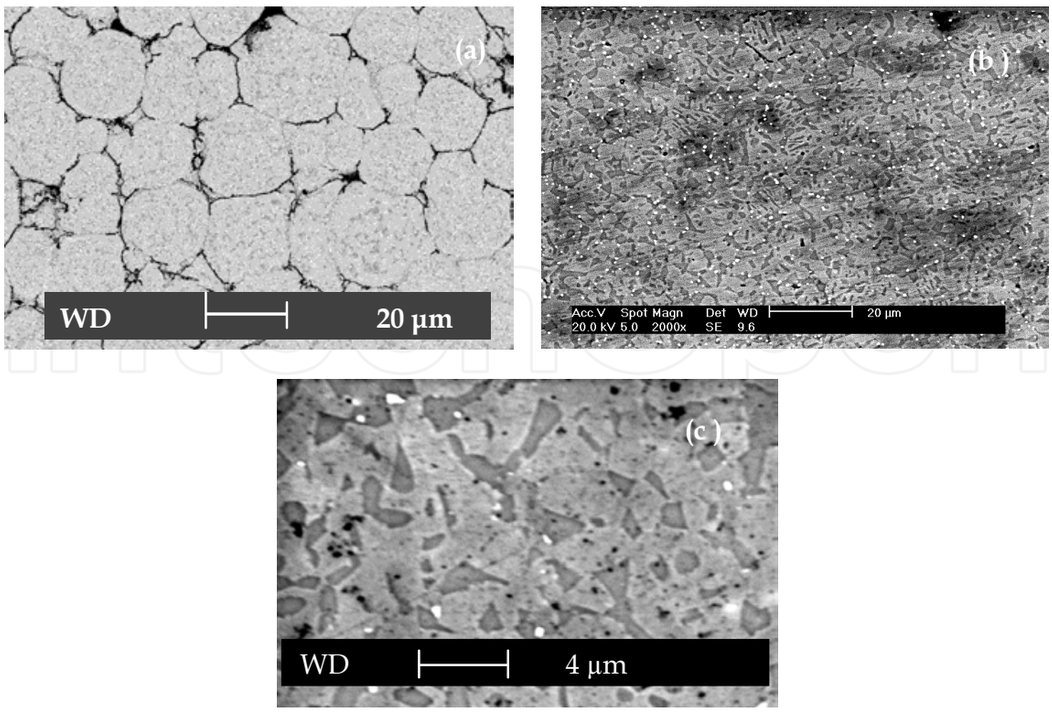

Fig. 13. Scanning electron micrograph of sintered sample by hot pressing;
(a) 1323 K- 30 minutes, (b) 1473 K-0 minutes and (c) 1473 K- 60 minutes respectively.

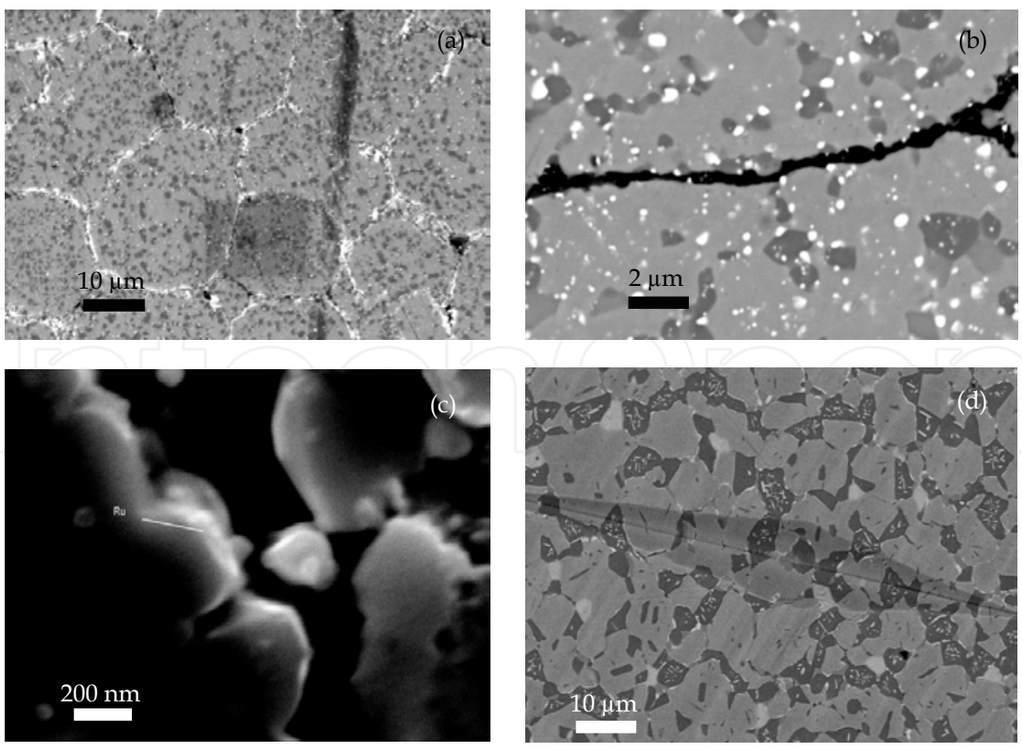

Fig. 14. Scanning electron micrograph of sintered sample Ru-doped by hot pressing;
(a) 1323 K- 30 minutes, (b) 1473 K-0 minutes and (c) 1473 K- 60 minutes respectively.

SIMS maps for 27Al and 99Ru of the same 50=50 mm2 area of the sintered doped sample are shown in Fig. 15. Bright zones in each map correspond to element rich phases, namely β-NiAl for the Al-rich zones. From a comparison of the two maps, it appears that Ru is found in β-NiAl. This re-organization is expected from the enhanced plasticity of β-NiAl in the sintering conditions, and is in agreement with literature information reporting that platinum group metals present a remarkable affinity for this phase β. Consequently, Fig. 15 reveals that sintering conditions allow Ru to diffuse completely from the outer surface to the core of the particles, towards the same position as it is expected to occupy in the bond coat. In view of this behavior, the same hot-pressing temperature 1473 K and duration of 1 h was selected for ensuring a complete densification and a reproducible microstructure.

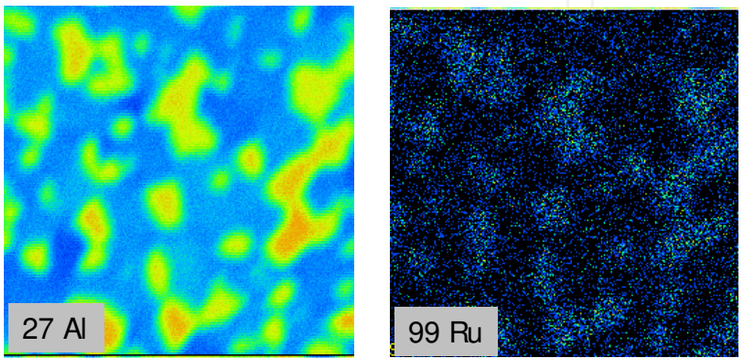

Fig. 15. ^{27}Al and ^{99}Ru SIMS maps of the same 50=50-mm2 area of the sintered MCrAlY doped sample.

4.2 Spark plasma sintering of MCrAlY powders undoped

SPS is found to be an effective technique to consolidate powder through the simultaneous application of direct pulsed current and uniaxial pressure (Munir et al., 2006). Assisted by an applied pressure, the electric current density induces a temperature elevation within the sample through the Joule´s effect, thus leading to powder sintering.

The emerging SPS theme from the large majority of investigations of current activated sintering is oriented to the advantages over conventional methods including pressureless sintering, hot-pressing, and others. These advantages include: lower sintering temperature, shorter holding time, and markedly improvements on the properties of materials consolidated by this method (Courat et al., 2008; Oquab et al., 2006).

The use of the hot-pressing techniques to optimize microstructure of MCrAlY alloys for high temperature application has been scarcely documented (Jeandin et al., 1988; Menzies et al., 1982; Somani et al., 1998; Prakash et al., 1988). The present study shows, the results of MCrAlY powder sintered by spark plasma sintering.

The SPS experiments were carried out on a commercial Dr Sinter Sumitomo 1050 apparatus (Sumitomo Coal Ming Co., Japan). This equipment can supply a direct current intense of 5000 Amp under a maximum voltage of 5 V. The powder was poured into a graphite die set of 20 mm wall thickness, placed between two graphite punches of 20 mm diameter (Fig. 16). Elements of graphite play both the role of electrodes and plates imparting the pressure. The sinter chamber is kept under vacuum (10^{-2} Pa) along the experiments.

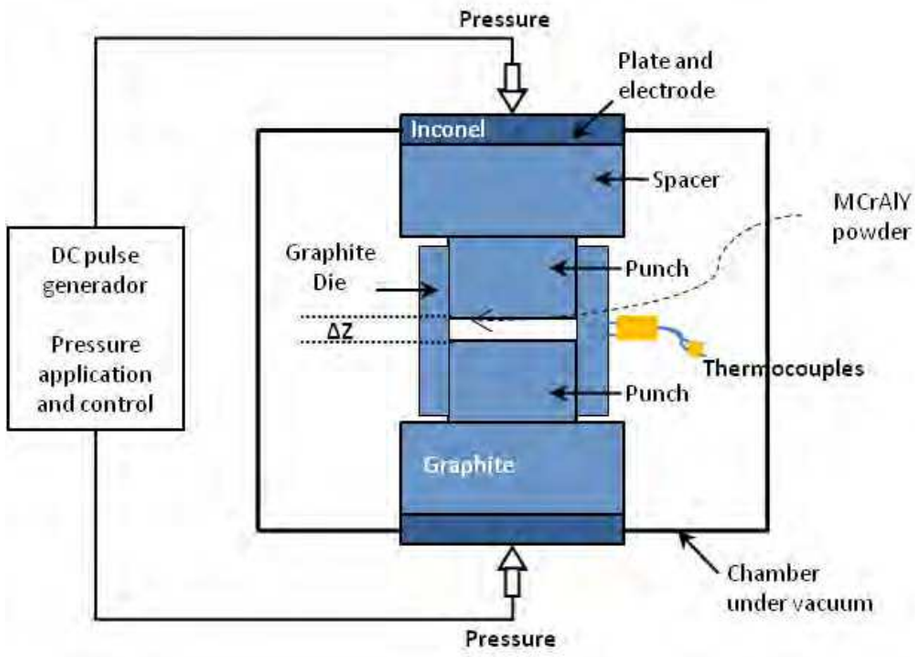

Fig. 16. Schematic illustration of the SPS technique.

MCrAlY alloy powders were consolidated at temperatures ranging between 1173 and 1323 K, range 15 KN in-load and processing time 0 and 30 minutes. To avoid grain coarsening of the microstructure of sintered specimen, SPS was conducted below the γ prime temperature, which is about 1140 °C (1413 K) (Prakash et al., 1988). The Fig. 17(a) shows an experimental record of the SPS-processing parameters, i.e., temperature, applied load and relative displacement of the punches, as a function of time. The relative displacement of the punches is expressed in percentage of the maximum displacement attainable. The temperature curve

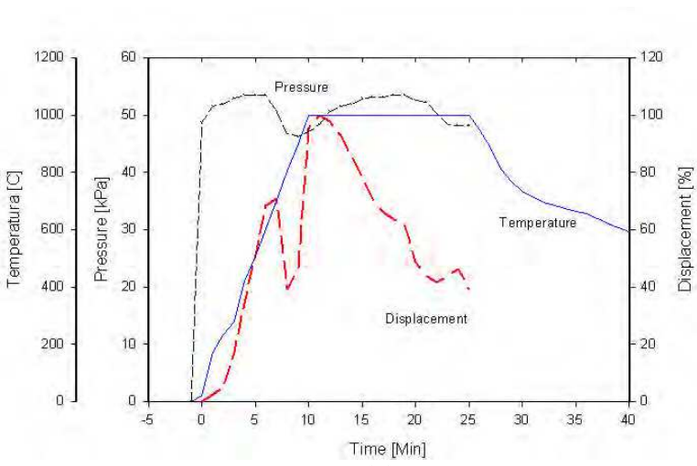

(a)

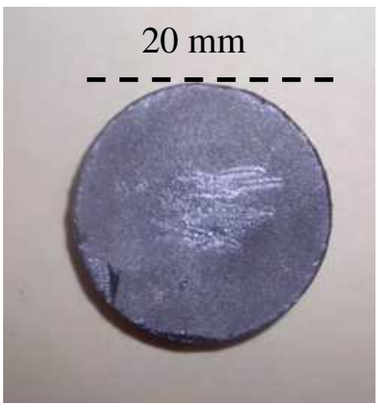

(b)

Fig. 17. Experimental record of a number of SPS-parameters such as; (a) Temperature, applied pressure and relative displacement of the punches as a function of time for an experiment MCrAlY performed at 1273 K. (b) Pastille obtained by SPS 20 mm diameter.

corresponds to the variation measured by the internal pyrometer. For this illustration, the selected holding temperature was 1273 K. Meanwhile pressure and current pulses are applied simultaneously. The set pressure was 50 KPa and was applied for 3 min. A heating rate of 150 °C/min was programmed, in such a way that the sintering temperature was reached in 9 minutes. After 15 minutes of holding time at the maximum temperature, the pressure and vacuum are then removed. This results in a pressure which falls quickly, whereas the temperature reduction takes 7 min to reach 600 °C. The cooling stage drop from 1000 to 600 °C occurs at a rate of 90 °C/min.

With above experimental parameters set the sintering of a tablet-like specimen of 20 mm diameter and 3 mm thick was accomplished in less than 15 minutes. No subsequent thermal treatment was applied to the tablets, in such a way that the final microstructure was obtained by one single step (Fig. 17(b)).

The Fig. 18 shows the microstructures of the MCrAlY alloys sintered at temperature of 1173, 1223, 1273 and 1323 K. SEM analysis of polished surfaces does not reveal presence porosity for the sintered samples at 1223 K, which confirms the major densification. Fig. 18(a) shows a surface of a sintered sample at 1173 K. At this sintering temperature, the surface still shows characteristics from original powder structure and is only observed one plastic deformation of the powders. For all temperatures, the microstructure is mainly composed of two phases, identified in a dark gray and light gray. EDS analysis on the sintered samples indicates that; dark gray area with high aluminum content would correspond to a β phase ($NiAl_3$), and the light gray area rich in nickel and chromium which would correspond to a γ phase nickel and, finally some rich precipitates in Tantalum would correspond to tantalum carbide TaC. The latter is shown in the analysis by energy dispersion spectroscopy.

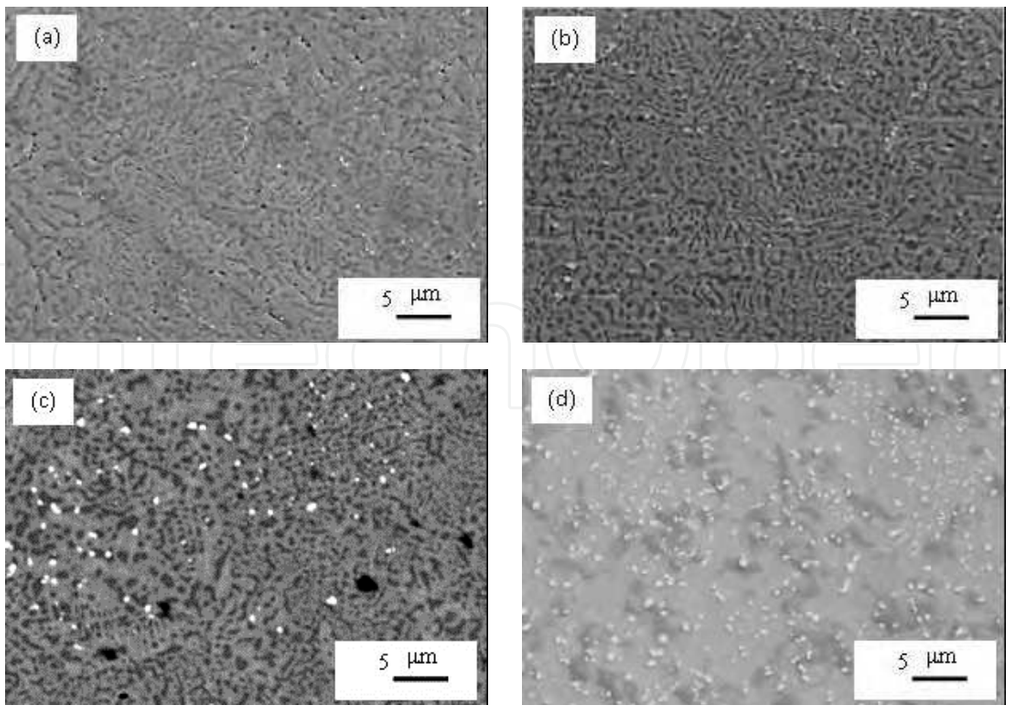

Fig. 18. Scanning electron micrographs of MCrAlY powder sintered by setting SPS at (a) 1173 K, (b) 1223 K, (c) 1273 K and (d) 1323 K.

Fig. 19 shows the XRD patterns evolution of the sintered MCrAlY. Two phases were identified: β $NiAl_3$ and γ Nickel. The set of conditions of temperature and pressure in SPS allowed to keep the same microstructure and grain coarsening is not appreciated at 1273 K.

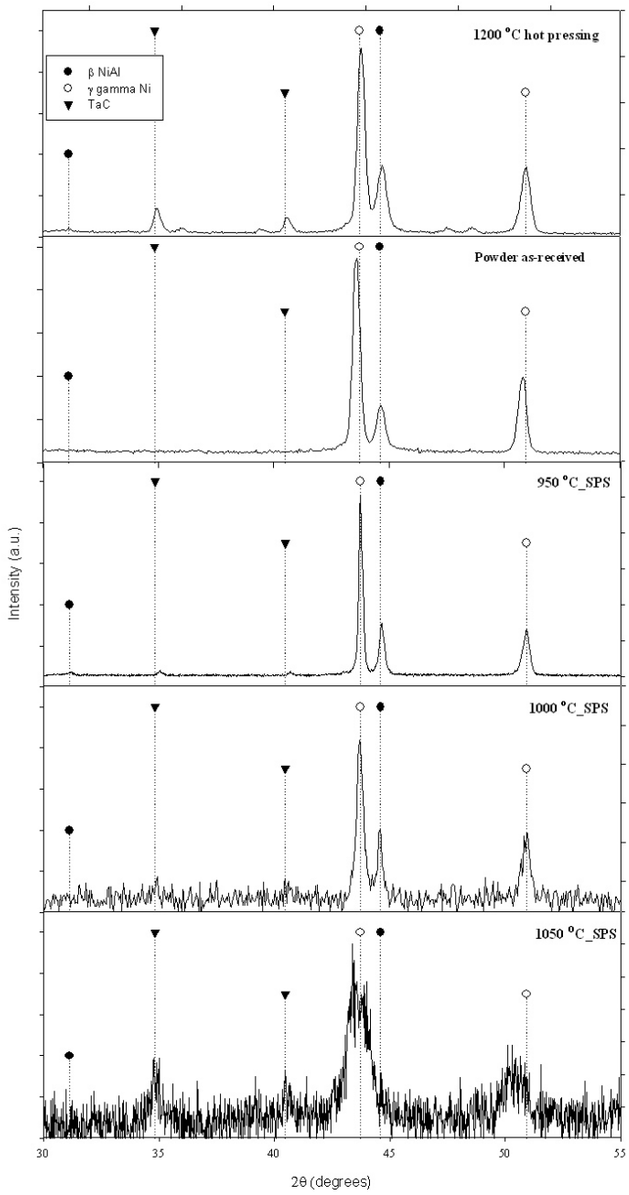

Fig. 19. XRD patterns for corresponding MCrAlY specimens sintered by SPS and hot pressing.

Fig. 20(a) shows the variation in porosity of sintered samples at different SPS temperatures between 1073 and 1323 K. A significant reduction in porosity is observed when an increasing sintering temperature is applied. Also this Fig. 20(b) shows an increasing Vickers hardness in function of SPS sintering temperature how effect of microstructural evolution. However, at temperature of 1323 K it is observed a diminution of hardness with a major porosity that could be associated with the start of the melting of components.

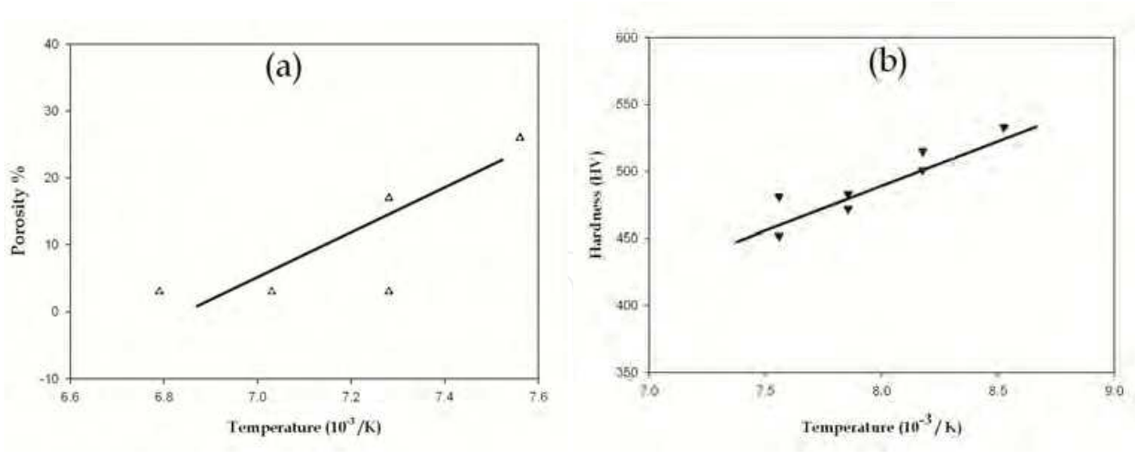

Fig. 20. Analysis of MCrAlY samples sintered by SPS for temperatures range between 1073 and 1273 K: (a) porosity (b) Vickers hardness.

To study the advantages of spark plasma sintering against hot pressing, Fig. 18(b) shows a secondary electron micrograph of surface of MCrAlY powders sintered by SPS. The present work clearly demonstrates that MCrAlY alloys can be rapidly sintered by SPS (in less than 30 min). As illustrated by the presence of little number of porosities, a full densification can be achieved by using SPS. From Fig. 6(b), both larger powder particles and a relative proportion of surface area/per volume unit limits the interstitial hardening, and tend to favor elastic deformation of powders. Moreover, the current density at contacts among larger particles should be higher because of a smaller number of connections and on other case of smaller particles the current density should be lower in where the sintering of powders started early, as it see at the Fig. 21. This shows a surface of MCrAlY sample sintered at 1173 K after a fracture procedure. Thus, a faster consolidation was achieved mainly due to the presence of a wide size distribution of powders allowing to fill the interstices present between the larger powders per the smaller ones.

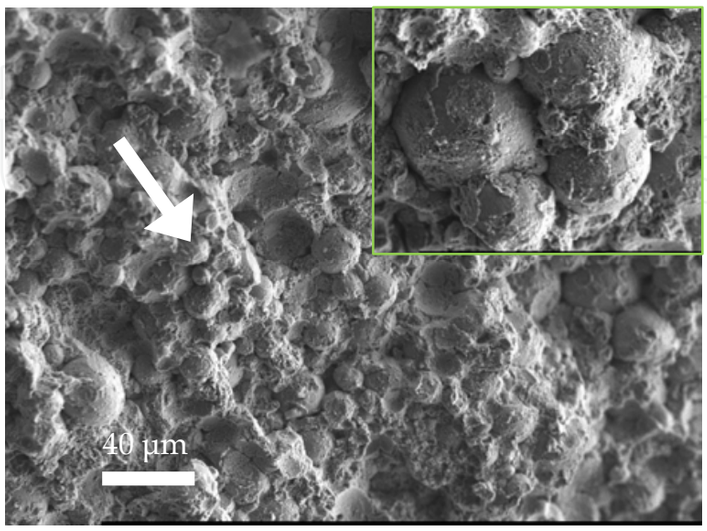

Fig. 21. Fracture surface of MCrAlY sample sintered at 1173 K.

Fig. 17(a) shows experimental record of a number of SPS parameters such as the densification of MCrAlY powders as function of time. During this period, grain boundaries were deformed and reorganized, especially due to the plastic deformation of the β phase rich in aluminum. In this Fig. 17(a), three main steps can be identified for the displacement variation, which could be interpreted as follows; in a beginning (5 min), when pressure increasing, the powder is compressed as a green body. This is followed by a flat stage. Sintering occurs in the final stage as the temperature reaches about 750 °C under 50 KN. For this condition, the pressure (applied load) exceeds the yield stress at a temperature below the brittle-ductile transition (950 °C). Then sintering begins taking place in less than 12 min. which means that full densification is achieved at a temperature of 950 °C, namely before the holding temperature has been reached. Finally the decrease of the relative displacement is interpreted as a result of the system dilation.

This latest β phase contains a major amount of aluminum, thus plastic deformation during the SPS process, is expected to be most important with respect to the presence of deformation in the γ phase that contains a major amount of nickel (Fig. 22). The measurement of the relative displacement of the punches (Fig. 17(a)) indicates that the compaction can be completed at 950 °C. Thus, as long as a transus temperature is not reached, a quite similar microstructure is generated. A short hold-time also helps to avoid grain ripening due to diffusion controlled by phase transformations. MCrAlY alloys might be satisfactorily described by a Ni-Al binary diagram with only a slight effect of Tantalum on the related transus temperature. The transus temperature for the Ni-Al alloys have been measured at 1100 °C, cf. (Noebe et al., 1993). Fig. 22 presents a backscattered scanning electron micrograph of a polished surface of sintered sample. Two phases, shown in dark gray and light gray, are present corresponding to β-NiAl and to γ-Ni, respectively. Tantalum carbide is detected for positions in white dots that also appear in this micrograph. For SPS temperatures ranging between 1173 and 1273 K two mainly phases are formed in the microstructure: β and γ. The SPS temperatures sintering are lower than the α transus temperature and no grain coalescence is observed due to the short duration of the experiments.

Contact among surfaces is favoring during SPS and the resulting product is exempt of open porosity. Fig. 18 shows the microstructures of the MCrAlY alloy sintered at SPS temperatures of 1173, 1223, 1273 and 1323 K. SEM analyses of polished surfaces do not reveal a porosity, which confirms a major compaction. Munir et al. (Munir et al., 2006) have not reported contribution of the time in the process consolidation of materials treated by SPS, from here for time range sintering between 0 min and 15 min, the MCrAlY alloy shows a similar microstructure of individual grains.

XRD diffraction patterns (Fig. 19) reveal the presence of an γ phase and an β phase for all temperatures, and there is neither difference in the positions of the peaks nor new peaks indicating the formation of a new phase. Besides, according with the peak shape, it is suggested that there was not coarsening of grain in the temperature range of 1223-1273 K for all sintered samples.

Courat et al. have mentioned that the current density conditions prevailing during the SPS process (Courat et al., 2008) do not allow mass transport. Thus the Tantalum carbide located on the surface of atomized powder before sintering process, it remains during sintering

within the limits of powders, and is only transported by the powder limit, as is observed in Fig. 22 for all sintering temperatures. Indeed the Tantalum carbide has a high melting point.

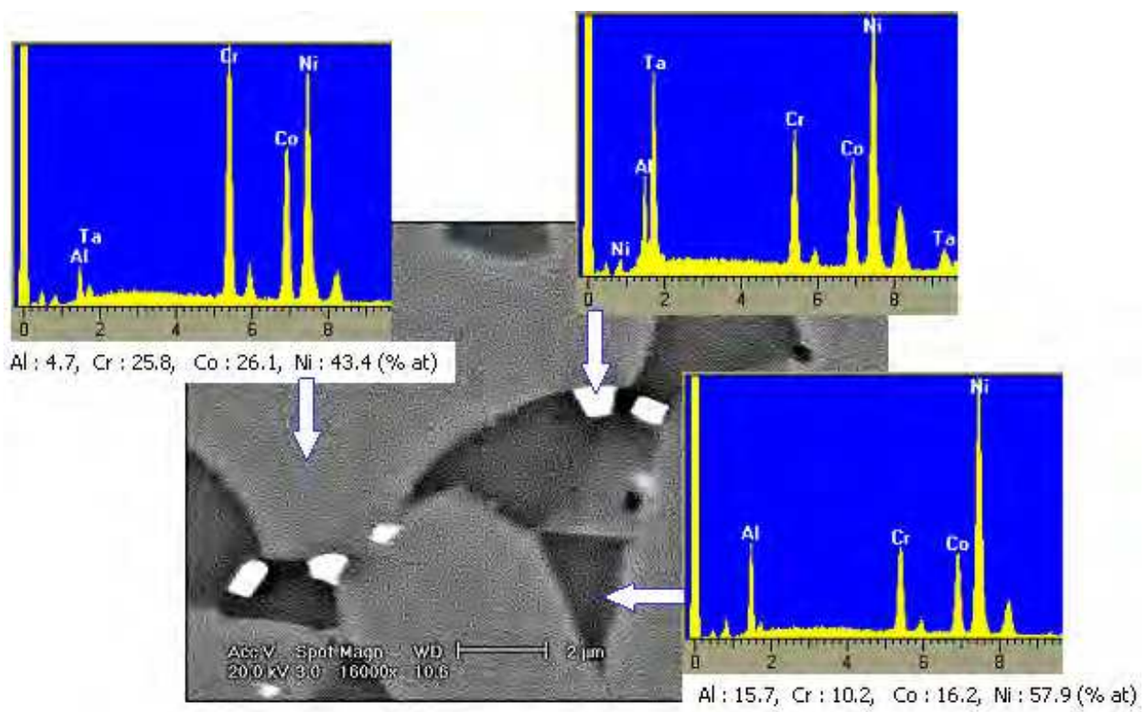

Fig. 22. Backscattered scanning electron micrograph of a polished surface of MCrAlY sintered sample at 1273 K.

5. Conclusions

Film characteristics show the SB-MOCVD process to be compatible with doping of MCrAlY powders prior to their use in the preparation of bond coats by sintering on turbine blades and vanes for improved mechanical and oxidation resistance during high temperature operation of gas turbines.

MCrAlY alloys were sintered by using hot-pressing and spark plasma sintering. For a temperature 1273 K and duration 30 min, specimens disclose a good compacting and a microstructure homogenous. Two phases in the microstructure are mainly formed under all sintering conditions: β Beta and γ gamma. Such, microstructures represents a real advantage by using spark plasma sintering with respect to hot-pressing conventional processing by a decrease of 200 ◦C degree in the sintering temperature. Indeed without any significant change in the structural and mechanical property.

However, the mechanical properties are still under investigation for SPS samples and it should be reported in the future.

Finally, spark plasma sintering process appears to be a promising route to produce MCrAlY alloys doped with Ruthenium and/or others materials.

6. Acknowledgments

The authors are grateful for the support to conduct this work to COFAA, EDI-IPN and CONACYT-SNI. And the authors are also indebted to Red de Nanotecnología of IPN, for the SPS facilities.

7. References

Alperine, S.; Steinmetz, F.; Josso, P. & Constantini, A. (1989). High temperature-resistant palladium-modified aluminide coatings for nickel-base superalloys. *Materials Science Engineering*. Vol. A121, pp 367-372, ISSN: 0921-5093.

Bose, S. & DeMasi-Marcin J. T. (1995). Thermal Barrier coatings experience in gas turbine engines at Pratt & Whitney, Workshop; *Thermal Barrier Coatings*, Cleveland Ohio, NASA CP 3312. pp. 63-77.

Caussat, B.; Juarez, F. & Vahlas C. (2006). Hydrodynamic study of fine metallic powders in an original spouted bed contactor in view of chemical deposition vapour treatments. *Powder Technology*. 135, pp. 63-70. ISSN 0032-5910.

Choi, S.R.; Zhu, D. & Miller, R.A. (1998). High-temperature slow crack growth, fracture toughness and room-temperature deformation behavior of plasma-sprayed ZrO2-8 wt % Y2O3. *Ceramic Engineering and Science proceedings*. Vol. 19, No 4, 293-301, ISSN 01966219.

Christensen, R.J.; Tolpygo, VK. & Clarke, DR. (1997). The influence of the reactive element yttrium on the stress in alumina scales formed by oxidation. *Acta Materialia*. Vol. 45, No. 4, pp. 1761-1766, ISSN: 1359-6454

Courat, A.; Molenat, G. & Galy, J. (2008). Microstructures and mechanical properties of TiAl alloys consolidated by spark plasma sintering. *Intermetallics*. Vol. 16, pp. 1134-1141, ISSN 0966-9795.

Cruse, TA.; Stewart, SE. & Ortiz, M. (1988): Thermal Barrier Coating Life Prediction Model Development. *Journal of Engineering for Gas Turbines and Power.* Vol. 110, pp. 610-616, ISSN 0742-4795.

Czech, N.; Schmitz, F. & Stamm, W. (1995). Microstructural Analysis of the Role Rhenium in Advanced MCrAlY Coatings. *Surface and Coatings Technology.* Vol. 76 - 77, pp. 28 - 33. ISSN 0257-8972.

Czech, N.; Schmitz, F. & Stamm, W. (1994). Improvement of MCrAlY coatings by addition of rhenium. *Surfaces and Coatings Technology*. Vol. 68-69, pp. 17-21, ISSN 0257-8972.

DeMasi-Marcin, J.T. & Gupta D. K. (1994). Protective coatings in the gas turbine engine. *Surfaces and Coatings Technology*. Vol. 68/69, pp. 1-9, ISSN 0257-8972.

DeMasi-Marcin, J.T.; Sheffler, KD. & Bose, S. (1990). Mechanisms of Degradation and Failure in a Plasma-Deposited Thermal Barrier Coating. *Journal of Engineering for Gas Turbines and Power*. October 1990 --Volume 112, Issue 4, pp. 521- 526, ISSN 0742-4795.

Eaton, H. E. & Novak, R. C. (1987). Sintering studies of plasma-sprayed zirconia. *Surface and Coatings Technology*. Vol. 32, pp. 227-236, ISSN 0257-8972.

Feng, Q. Nandy, T.K. Tin, S. & Pollock, T. (2003). Solidification of high-refractory ruthenium -containing superalloys. *Acta Materialia* 51 (1) (2003), pp. 269-284, ISSN 1359-6454.

Fleischer, R.L.; Field, R.D. & Briant, C.L. (1991). Mechanical properties of high-temperature alloys of AlRu. *Metallurgical Transactions A*. Vol. 22A, pp. 403-414, ISSN 1073-5623.

Golightly, F.A.; Sttot, F.H. & Wood, G.C. (1976). The influence of yttrium additions on the oxide-scale adhesion to an iron-chromium-aluminum alloy. *Oxidation of Metals*. Vol. 10, No. 3 pp. 163-187, ISSN 0030- 770X.

Haynes, J.A.; Zhang, Y.; Lee, W.Y.; Pint, B.A.; Wright, I.G. & Cooley, K.M. (1999). Effects of Pt Additions and S Impurities on the Microstructure and Scale Adhesion Behavior of Single-Phase CVD Aluminide Bond Coatings Hampikian JM, Dahotre NB, editors. *Elevated temperature coatings: science and technology III, Symposium Proceeding Warrendale* (PA) TMS, pp. 185-196, ISBN 0873394216.

Hillery R. editor. (1996) NRC report. Coatings for high temperature structural materials: Trends and opportunities. *National Academy Press*, pp 43-45, ISBN-10: 0-309-08683-3.

Jeandin, M.C.M. Koutny, J.-L. & Bienvenu, Y.C. (1988). Procédé d'Assemblage de Piéces en Superalliages à base de Nickel par Frittage en Phase Liquide et Compaction Isostatique à Chaud, *Institut National de la Propiété Industrielle*, France, 2610856 Patent. (2610856).

Juarez, F.; Castillo, A.; Pieraggi, B. & Vahlas, C. (2001) Spouted bed metallorganic chemical vapor deposition of ruthenium on MCrAl-Y powders. *Journal de Physique IV*. Vol. 11, pp. 1117-1123. ISSN 1155-4339.

Juarez, F.; Lafont, M-C.; Senocq, F. & Vahlas, C. (2005). Spouted bed of MCrAlY powders in applications CVD. *Electrochemical Society Proceeding*, No. 08, pp. 501-508, ISBN 978-1-56677-793-3

Juarez, F.; Monceau, D.; Tetard, D.; Pieraggi, B. & Vahlas, C. (2003), Chemical vapor deposition of ruthenium on NiCoCrAlYTa powders followed by thermal oxidation of the sintered coupons. *Surfaces and Coatings Technology*, Vol. 163-164, pp. 44- 49. ISSN 0257-8972.

Kingery, W.D.; Bowen H.K. & Uhlmann, D.R. (1976) Introduction to ceramics. New York: *Wiley and Sons,* pp. 1056. ISBN0471478601.

Lee, EY. & Sisson, R.D. (1994). The effect of bond coat oxidation on the failure of thermal barrier coating: thermal spray industrial applications In: Berndt CC, Sampath S. editors. Proc. *7th National Spray Conference, Boston* MA, 20-24 June. Materials Park, OH: ASM International, pp. 55-59. ISBN 0871705095.

Lipkin, D.M. & Clarke, D.R. (1996), Measurement of the stress in oxide scales formed by oxidation of alumina-forming alloys. *Oxidation of Metals*. Vol. 45, No. 3-4, pp. 267-280. ISSN 0030-770X.

Lu D.C. & Pollock, T.M. (1999). Low temperature deformation and dislocation substructure of ruthenium aluminide polycrystals. *Acta Materialia.* Vol. 47 No. 3, pp. 1035-1042, ISSN 1359-6454.

Lu, D.C. & Pollock, T.M. (1999). Low temperature deformation kinetics of ruthenium aluminide alloys. *Material Research Society Symposium Proceedings*. Vol. 552, pp. KK7.11.1-KK7.11.5, ISSN 02729172. Symposium KK - High-Temperature Ordered Intermetallic Alloys VIII , MRS Fall Meeting, Boston MS, USA, 1998.

Mariochocchi, A.; Bartz, A. & Wortman, D. (1995). PVD TBC Experience on GE Aircraft Engines. In *proceedings 1995 Thermal Barrier coatings workshop* W. J. Brindley, Ed., NASA CP 3312. pp. 79-89.

Meier, G.H. & Pettit, F.S. (1999). Interaction of steam/air mixtures with turbine airfoils alloys and coatings. Report on AFOSR Contract F49620-981-0221. Univ. of Pittsburgh, 1 September, pp. 1-9.

Meier, S.M.; Nisseley, D.M. & Sheffer, K.D. (1991) Thermal barrier coating life prediction model development phase II. NASA CR-18911, July.

Meier, SM. & Gupta, D.K. (1994). The evolution of thermal barrier coatings in gas turbine engine applications. *Journal of Engineering for Gas Turbines and Power, Trans ASME,* vol. 116, No. 1, pp. 250-257, ISSN 0742-4795, January 1994.

Mennicke, C.; Schumann, E.; Ulrich, C. & Ruehle, M. (1997). The Effect of Yttrium and Sulfur on the Oxidation of FeCrAl. *Materials Science Forum*. Vol. 251-254, pp. 389-396, ISSN: 1662-9752.

Menzies, R.G.; Davies, G.J. & Edington. J.W. (1982). Effect of the Treatment on Superplastic Response of Powder - Consolidated nickel - Base Superalloy IN100. *Metal Science.* Vol. 16, No. 7, pp. 356-362, ISSN 0306-3453.

Miller, R.A. (1984). Oxidation-Based Model for Thermal Barrier Coating Life. *Journal American Ceramic Society*. Vol. 67, No. 8, C-154-C 170 pp. 517-521, ISSN 1551-2916.

Monceau, D.; Boudot-Miquet, A.; Bouhanek, K.; Peraldi, R.; Malie, A.; Crabos, F. & Pieraggi, B. (2000), Oxydation et protection des matériaux pour sous -couches (NiAlPd, NiAlPt, NiCoCrAlTa, CoNiCrAlY) de barrières thermiques, *Journal Physical IV* France 10, pp. 167-171, ISSN 1155-4339.

Munir, Z. A.; Anselmi -Tamburini U. & Ohyanagi, M. (2006). The effect of electric field and pressure on the synthesis and consolidation of materials: A Review of the spark plasma sintering method. *Journal of Materials Science*. Vol. 41, pp. 763-777, ISSN 0022-2461.

Nickel, H.; Clemens, D.; Quadakkers, W.J. & Singheiser, L. (1999). Development of NiCrAlY Alloys for Corrosion - Resistant Coatings of Gas Turbine Components. *Journal of Pressure Vessel Technology*. Vol. 121, pp. 384-387, ISSN 0094-9930.

Noebe, R.D.; Bowman, R.R. & Nathal, M.V. (1993). Physical and mechanical properties of the B2 compound NiAl. *International Materials Reviews.* Vol. 38 No. 4, pp. 193-232. ISSN 0950-6608.

Oquab, D.; Estournes, C. & Monceau, D. (2006). Oxidation resistant aluminized MCrAlY coating prepared by Spark Plasma Sintering (SPS). *Advanced Engineering Materials*. Vol. 9, No. 5, pp. 413-417, ISSN 1527-2648.

Pollock, T.M.; Lu, D.C.; Shi, X. & Eow, K. (2001). A comparative analysis of low temperature deformation in B2 aluminides. *Materials Science and Engineering A*. Vol. 317 No. 1-2, pp. 241-248, ISSN 0921-5093.

Prakash, T. L.; Somani M.C. & Bhagiradha Rao, E.S. (1988). Structure property correlation of as- HIPped and HIP + forged P/M alloy nimonic AP-1, *Powder Metallurgy Related High Temperature Materials*. Vol. 29-31, pp. 179-198, ISBN 978-0-87849-577-1

Quadakkers, WJ.; Tyagi, AK.; Clemens, D.; Anton, R. & Singhesir, L. (1999). The Significance of Bond Coat Oxidation for the Life of TBC Coatings. Hampikian JM, Dahotre NB, editors. *Elevated temperature coatings: science and technology III, Symposium Proc., Warrendale* (PA) TMS, pp. 119-130, ISBN 0873394216.

Rigney, D.V.; Viguie, R.; Wortman, D.J. & Skelly, W.W. (1995). PVD thermal barrier coatings applications and process development for aircraft engines, *in Proc of the workshop on Thermal Barrier Coatings, NASA-CP-3312*. NASA Lewis Research Center, pp. 135-150.

Sarioglu, C. ; Blachere, JR. ; Petit FS, & Meier, GH. (1997). Room temperature and in situ high temperature strain (stress) measurements by XRD techniques. *Proceedings of the Third International Conference held at Trinity Hall,* Cambridge 1996In: Newcomb S.B. Little J.A. Editors. London: Microscopy of oxidation Vol. 3. The institute of materials, pp. 41-51, ISBN: 9781861250346.

Schaeffer, J.; Kim, G.M.; Meier, G.H. & Pettit, F.S. In: Lang E. editors. (1988). *Proceeding of the European Colloquium*; The role of the active elements in the oxidation behavior of the high temperature metals and alloys: The effects of precious metals on the oxidation and hot corrosion of coatings. Elsevier Applied Science pp. 231-270. ISBN: 1-85- 166-420-3.

Sergo, V. & Clarke, D.R. (1998). Observation of Subcritical Spall Propagation of a Thermal Barrier Coating. *Journal American Ceramic Society*. Vol. 81, No. 12, pp. 3237-3242, ISSN 1551-2916.

Shiojiri, M.; Kawasaki, M.; Fujii, M.; Wakayama, M. & Yoshioka, T. (1999). High-resolution transmission electron microscopy of Fe-Al powder particles. *Journal Electron Microscopy*. Vol. 48, No. 4, pp. 367- 373, ISSN 0022-0744.

Smegil, J.G. (1987). Some comments on the role of yttrium in protective oxide scale adherence. *Materials Science Engineering*. Vol. 87, pp. 261-265, ISSN: 0921-5093.

Smialek, J.L.; Jayne, D.T.; Schaeffer, JC. & Murphy, WH. (1994). Effects of hydrogen annealing, sulfur segregation and diffusion on the cyclic oxidation resistance of superalloys: a review. *Thin Solid Films*, Vol. 253, No. 1-2, pp. 285-292, ISSN 0040-6090.

Somani, M.C.; Muraleedharan, K.; Prasad, Y.V. & Sigh, V. (1998). Mechanical Processing and Microstructural Control in hot Working of hot Isostatically Pressed P/M IN-100 Superalloy. *Materials Science and Engineering* A. Vol. 245, pp. 88-99, ISSN 0921-5093.

Stiger, M.J.; Yanar, N.M.; Topping, MG.; Pettit, F.S. & Meier, GH. (1999), Thermal Barrier coatings for the 21st century, *Z. Metallkd*. Vol. 90, No. 12, pp. 1069-1078. ISSN 0044-3093.

Strangman T.E. (1985), Thermal barrier coatings for turbine airfoils. *Thin Solid Films*. Vol. 127, pp. 93-106, ISSN 0040-6090.

Taylor, T.A.; Bettridge, D.F.; Tucker, Jr. & Robert, C. (1995). Coating composition having good corrosion and oxidation resistance Praxair S.T. Technology, Inc. Rolls-Royce PLC, *USA Patent* 5455119, October 1993.

Taylor, T.A. & Bettridge, D.F., (1996). Development of Alloyed and Dispersion-Strengthened MCrAlY Coatings. *Surface and Coatings Technology*, Vol. 86- 87, pp. 9-14, ISSN 0257-8972.

Tolpygo, V.K. & Clarke, D.R. (1998). Competition Between Stress Generation and Relaxation During Oxidation of a Fe-Cr-Al-Y Alloy. *Oxidation of Metals*. Vol. 49, No 1-2, pp. 187-211. ISSN 0030-770X.

Tolpygo, VK. & Clarke, DR. (1998) Wrinkling of α-alumina films grown by thermal oxidation-I. Quantitative studies on single crystals of Fe-Cr-Al alloy. *Acta Materialia*. Vol. 46, No. 14, pp. 5153-5166, ISSN 1359-6454

Tryon, B.; Cao, F.; Murphy, K.S.; Levi, C.G. & Pollock, T.M. (2006). Ruthenium-containing bond coats for thermal barrier coating systems. Journal of Metals. Vol. 58 No. 1, pp. 53-59, ISSN 0148-6608.

Tryon, B.; Pollock, T.M.; Gigliotti, M.F. & Hemker, K. (2004) Thermal expansion behavior of ruthenium aluminides. *Scripta Materialia*. Vol. 50, No. 6, pp. 845-848, ISSN 1359-6462

Vahlas, C.; Juarez, F.; Feurer, R.; Serp, P. & Caussat, B. (2002), Chemical vapor deposition on fluidized particles; Application to the metalorganic CVD of platinum group metals. *Adv. Mater. - Chemical Vapour Deposition*, Vol. 8, No. 4, pp. 127-143, ISSN 0948-1907.

Van de Voorde, M. H. & Meetham, W. G. (2000). Materials for High Temperature *Engineering Applications, Springer-Verlag*, Berlin, pp. 0-173, ISBN: 3540668616, ISBN-13: 97835406686192000.

Wang, Y.; Guo, H.; Peng, H.; Peng, L. & Gong, S, (2011), Diffusion barrier behaviors of (Ru,Ni)Al/NiAl coatings on Ni-based superalloy substrate. Intermetallics, *Proceedings of the 7th International Workshop on Advanced Intermetallics and Metallic Materials* 2008, Volume 19, Issue 2, February 2011, pp 191-195, ISSN 0966-9795.

Wolff, I.M. & Sauthoff, G. (1996), Mechanical properties of Ru-Ni-Al alloys. *Metallurgical and Materials Transactions A: Physical Metallurgy and Materials Science.* Vol. 27A, No. 5, pp. 1395-1400, ISSN 1073-5623.

Wolff, I.M. (1997). Toward a better understanding of ruthenium aluminide. *Journal of Metals*. 49 (1) (1997), pp. 34-39, ISSN 0148-6608.

Wright PK, (1998), Influence of cyclic strain on life of a PVD TBC. *Materials Science and Engineering A.* Vol. 245, pp. 191-200, ISSN 0921-5093.

Wright, P.K. & Evans, A.G. (1999). Mechanisms governing the performance of thermal barrier coatings. *Current Opinion in Solid State and Materials Science*. Vol. 4, No. 3, pp. 255-265, ISSN 1359-0286.

Yoshioka, T.; Kawasaki, M.; Kitano, M.; Nishio, K. & Shiojiri, M. (1995), Cross-Sectional Transmission Electron Microscopy of ZnO Tetrapod-Like Particles, *Journal Electron Microscopy*, Vol. 44, No. 6, pp- 488-492, ISSN 0022-0744.

Yoshioka, T.; Kawasaki, M.; Yamamatsu, J.; Nomura, T.; Isshiki, T. & Shiojiri, M. (1997). A preparation method of sections of fine particles and cross-sectional transmission electron microscopy of Ni powder. *Journal Electron Microscopy*. Vol. 46, No. 4, pp. 293-301, ISSN 0022-0744.

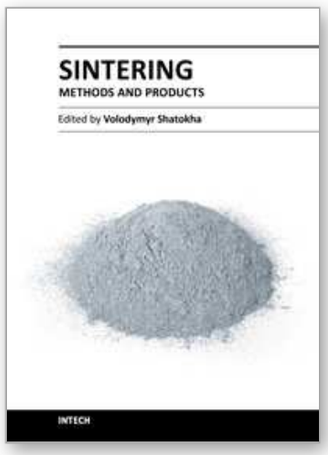

Sintering - Methods and Products

Edited by Dr. Volodymyr Shatokha

ISBN 978-953-51-0371-4
Hard cover, 316 pages
Publisher InTech
Published online 23, March, 2012
Published in print edition March, 2012

This book is addressed to a large and multidisciplinary audience of researchers and students dealing with or interested in sintering. Though commonly known as a method for production of objects from fines or powders, sintering is a very complex physicochemical phenomenon. It is complex because it involves a number of phenomena exhibiting themselves in various heterogeneous material systems, in a wide temperature range, and in different physical states. It is multidisciplinary research area because understanding of sintering requires a broad knowledge - from solid state physics and fluid dynamics to thermodynamics and kinetics of chemical reactions. Finally, sintering is not only a phenomenon. As a material processing method, sintering embraces the wide group of technologies used to obtain such different products as for example iron ore agglomerate and luminescent powders. As a matter of fact, this publication is a rare opportunity to connect the researchers involved in different domains of sintering in a single book.

INTECH
open science | open minds

InTech Europe
University Campus STeP Ri
Slavka Krautzeka 83/A
51000 Rijeka, Croatia
Phone: +385 (51) 770 447
Fax: +385 (51) 686 166
www.intechopen.com

InTech China
Unit 405, Office Block, Hotel Equatorial Shanghai
No.65, Yan An Road (West), Shanghai, 200040, China
中国上海市延安西路65号上海国际贵都大饭店办公楼405单元
Phone: +86-21-62489820
Fax: +86-21-62489821

IntechOpen